Pramana – J. Phys. (2019) 93:74
https://doi.org/10.1007/s12043-019-1834-z

Successive linearisation approach to analyse thermally radiative stagnation point micropolar nanofluid flow with regression model

B KUMAR[1,*], G S SETH[1] and R NANDKEOLYAR[2]

[1]Department of Applied Mathematics, Indian Institute of Technology (Indian School of Mines), Dhanbad 826 004, India
[2]Department of Mathematics, National Institute of Technology, Jamshedpur 831 014, India
*Corresponding author. E-mail: chauhanbhuvan6@gmail.com

MS received 12 March 2019; revised 4 May 2019; accepted 9 May 2019

Abstract. The present paper is devoted to the investigation of magnetohydrodynamics (MHD) mixed convection stagnation point flow of a micropolar nanofluid with thermal radiation, microrotation, viscous and Joule dissipations, Brownian and thermophoretic diffusions, etc. The present analysis is done because it contains large potential to deal with many industrial processes such as electrical power generation, nuclear energy plant, melt spinning technique for cooling liquids, astrophysical flows, space vehicles, geothermal extractions, solar system, etc. The numerical solutions of the governing equations are obtained by successive linearisation method (SLM). The influence of various developing parameters, such as thermal radiation parameter, mixed convection parameter, thermophoretic parameter, etc., on the flow field is examined through graphs by accumulating sufficient data using SLM. A comparative study is performed between our results and previously obtained results in the limiting sense. Apart from this, the quadratic multiple regression analysis is performed for skin friction coefficient. It indicates that when the free stream is moving with less velocity than stretching velocity then a small variation in microrotation leads to large perturbation in skin friction in comparison to mixed convection parameter but in the opposite case, the buoyancy force becomes more dominant.

Keywords. Quadratic multiple regression analysis; thermophoretic and Brownian diffusions; thermal radiation; viscous and Joule dissipations; successive linearisation method.

PACS Nos **47.85.ld; 47.65.−d; 47.55.Ca; 47.55.P**

1. Introduction

A nanofluid is a fluid having nanometre-sized particles, called nanoparticles. Many researchers are attracted to the investigation of new models of nanofluid flow for the last two decades. The basic theory of a fluid containing a suspension of nanometre-sized particle is initially presented by Choi and Eastman [1]. The nanoscale particles are normally made of oxides, carbides (a more electropositive element) and metals. Nanofluid plays crucial role in many fields such as chemical science, environmental science, electronics, nuclear system, industries, medical science, etc. due to its higher thermal conductivity, minimal clogging properties and long-term stability. The strange increment in the thermal conductivity of nanofluid is first presented by Masuda *et al* [2]. Buongiorno [3] observed that thermal dispersion, thermal conductivity and intensified turbulence encountered by the motion of nanoparticles play a significant role in the increment of heat transfer of nanofluid. Kuznetsov and Nield [4] found that it is impossible to keep the volume fraction of nanoparticles constant at the surface. Therefore, they introduced a zero mass flux of nanofluids and investigated the boundary layer flow of nanofluids with natural convection. Some useful and innovative studies on nanofluids are presented by researchers [5–10].

The investigation of non-Newtonian fluid has received great attention due to its wide applications in designing procedures, numerous organic compounds, power system dynamics and medical sciences. Eringen [11] was the first to explain the theory of microrotation and high orientation of micropolar fluid particles. It is well known that Navier–Stokes theory cannot fully describe the behaviour of micropolar fluid due to its exotic nature. Eringen [12] further extended his work to describe the

Published online: 08 August 2019

theory of thermomicropolar fluid. The application of micropolar fluid in various fields and the explanation of mathematical equation of micropolar fluid in various situations are presented in the book by Lukaszewicz [13]. Heat transfer characteristics of micropolar fluid flow over stretchable surface in the presence of viscous dissipation and heat absorption are investigated by Mohammadein and Gorla [14]. Ibrahim *et al* [15] studied the influence of thermal relaxation time on angular velocity and proposed a model for micropolar fluid to notice thermal effect on the Stokes second problem. Sheikholeslami *et al* [16] used the analytical method to study the heat transfer of micropolar fluid in a permeable channel and described the effect of chemical reaction on the micropolar fluid flow. Uddin *et al* [17] proposed a fascinating model on micropolar fluid flow from a moving plate by using the Lie group transformation and taking thermal slip boundary condition. Iram *et al* [18] investigated the effects of temperature and concentration gradients on heat and mass transfer in micropolar fluid.

Flow adjacent to stretching sheet is of high concern for researchers due to its use in many engineering and industrial fields. Several applications of these models are widely used in manufacturing long and uniform metal parts, melt spinning technique for cooling liquid, metalworking process such as hot rolling, rubber sheets, elastic polymer substance, corrosion-resistant fabrics, and production of emollient, paints, glass fibre for thermal insulation, etc. Initially, Crane [19] examined the solution of boundary layer equations of Newtonian fluid over a stretching sheet. Kandasamy *et al* [20] carried out the investigation regarding magnetohydrodynamics (MHD) flow of the nanofluid over a stretching sheet. Turkyilmazoglu [21] studied the flow of micropolar fluid due to a permeable stretchable surface. Hsiao [22] proposed a fascinating model of stretching sheet problem regarding micropolar nanofluid flow by considering the effect of viscous dissipation. Nanofluid flow over a stretching surface under convective boundary conditions and temperature-dependent fluid viscosity has been numerically investigated by Afify and El-Aziz [23].

Natural convection is a process in which fluid motion is dependent on density difference in the fluid, encountered due to temperature gradients. Free convection plays a crucial role in nanofluid flow because nanofluid has high thermal conductivity. Forced convection is a process in which fluid motion is developed by external sources like fan, pump, etc. When these two mechanisms occur simultaneously, then it is termed as mixed convection and used in many thermal engineering processes. Khanafer *et al* [24] studied the buoyancy-driven flow by utilising Cu–water nanofluid and described the correlation for Nusselt number. Hassanien *et al* [25] studied the natural convective micropolar fluid flow and observed that micropolar fluid increases skin friction and tends to decrease the heat transfer. MHD stagnation point flow with buoyancy effect is studied by Makinde *et al* [26] by taking viscous and Joule dissipations into account and they reported that in the case of shrinking sheet, dual solution exists. They also found that skin friction decreases while Nusselt number increases with the enhancement in buoyancy force. Waqas *et al* [27] studied the heat transfer characteristics of micropolar fluid flow by using convective boundary conditions and taking nonlinear stretching sheet. Das [28] described the slip effect on MHD micropolar fluid stagnation point flow using the shrinking vertical surface. Bourantas and Loukopoulos [29] studied another model based on micropolar nanofluid with natural convection in order to examine the influence of magnetic field within the inclined rectangular cavity.

Stagnation point flow has immense use in many fields such as manufacturing of plastic substance, metallurgy, lubricant polymer extrusion, etc. Therefore, so many researchers moved towards analysing the boundary layer effect near the stagnation point. Viscous dissipation and Joule heating are very important for various energy efficient systems because they have the potential to alter the performance of the system. Bachok *et al* [30] described the MHD stagnation point flow of nanofluid by taking copper, alumina and titania as nanoparticles. Ibrahim *et al* [31] described the impact of various physical entities such as thermophoretic, Brownian motion and magnetic field on MHD stagnation point flow and observed that skin friction coefficient increases with the enhancement in stretching rate. Mahmood *et al* [32] used the Chebyshev spectral scheme to examine the dual solution of hydromagnetic Hiemenz stagnation point micropolar fluid flow. In order to examine the thermophysical property of micropolar fluid, Seth *et al* [33] investigated the mixed convection stagnation point flow towards a stretching surface. Azhar *et al* [34] investigated the stagnation point flow of a non-Newtonian fluid along with the Cattaneo–Christov heat flux model.

The heat transfer system is brilliantly modulated by thermal radiation. Thermal radiation effect is used in many scientific and engineering processes such as electrical power generation, nuclear energy plant, astrophysical flows, space vehicle, geothermal extractions, solar system, gas turbines, etc. Kim and Fedorov [35] used the Rosseland approximation to explain radiative heat transfer in micropolar fluid past a porous plate in the presence of thermal radiation field. Pal and Mandal [36] considered the impact of thermal radiation and proposed a model regarding the flow of micropolar fluid near a stretchable surface in the presence of transverse magnetic field. They studied the influence of microrotation and found that solid volume fraction

has opposite effect on fluid velocity. Siddiqa *et al* [37] proposed a fascinating model of micropolar fluid influenced by radiation and observed that heat transfer rate remains unaffected with the change in micropolar parameter. Hayat *et al* [38] described the impact of Brownian and thermophoretic diffusions on micropolar fluid flow over stretchable sheet influenced by radiation with the help of homotopy analysis method.

Our main purpose of addressing this model is to analyse the effects of thermal radiation, mixed convection, Joule and viscous dissipations, thermophoretic and Brownian diffusions on micropolar nanofluid stagnation point flow by considering suitable flow controlling parameters.

2. Mathematical formulation

The present system deals with the steady two-dimensional incompressible and electrically conducting stagnation point flow of micropolar nanofluid over a stretching sheet with mixed convection, thermal radiation, microrotation, viscous dissipation, Brownian motion, ohmic heating and thermophoretic effect. While deriving this model, it is assumed that nanoparticles and base fluid are in thermal equilibrium and also there is no chemical reaction between them. The induced magnetic field is neglected and the density variation obtained from concentration or temperature difference is neglected except in the case of thermal buoyancy force. It is also assumed that ambient fluid velocity $u_\infty = ax$ and stretching sheet velocity $u_w = bx$, where a and b are constants. The magnetic field is exerted perpendicular to the stretching sheet for controlling the boundary layer. T_∞ and T_w are the fluid temperatures in free stream and at the stretching sheet, respectively. Further, we have taken the x-axis along the surface of the sheet and the y-axis normal to it. The physical situation is chosen in such a way that when the nanofluid falls normally to the surface then sheet stretches linearly as $u_w = bx$. The geometry of the model is presented in figure 1. Nanoparticles volume fraction is taken according to Kuznetsov and Nield [39] at the surface, whereas species concentration in free stream is C_∞. Under these assumptions, the governing boundary layer equations, i.e. continuity, momentum, angular momentum, energy and concentration equations, are expressed, respectively, as follows:

$$\frac{\partial u}{\partial x} + \frac{\partial v}{\partial y} = 0, \tag{1}$$

$$u\frac{\partial u}{\partial x} + v\frac{\partial u}{\partial y} = \left(\upsilon_f + \frac{k_f}{\rho_f}\right)\frac{\partial^2 u}{\partial y^2} + \frac{k}{\rho_f}\frac{\partial N}{\partial y} + \frac{\sigma {B_0}^2}{\rho_f}(u_\infty - u) + u_\infty \frac{\mathrm{d}u_\infty}{\mathrm{d}x} + g\beta(T - T_\infty), \tag{2}$$

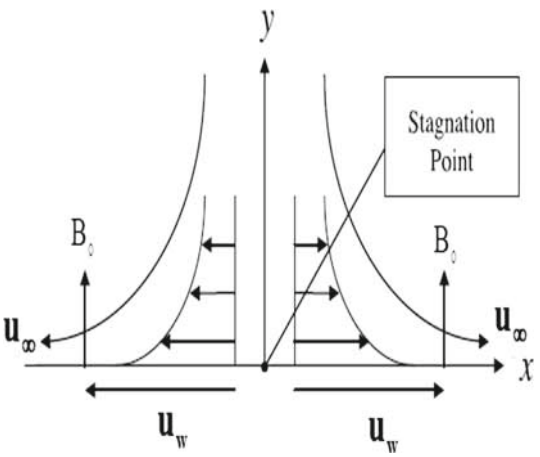

Figure 1. Geometry of the model.

$$u\frac{\partial N}{\partial x} + v\frac{\partial N}{\partial y} = \frac{\gamma_f}{(j\rho)_f}\frac{\partial^2 N}{\partial y^2} - \frac{k}{(j\rho)_f}\left(2N + \frac{\partial u}{\partial y}\right), \tag{3}$$

$$u\frac{\partial T}{\partial x} + v\frac{\partial T}{\partial y} = \frac{k_f}{(\rho c_p)_f}\frac{\partial^2 T}{\partial y^2} + \frac{(\mu_f + k_f)}{(\rho c_p)_f}\left(\frac{\partial u}{\partial y}\right)^2 + \frac{\sigma B_0^2}{(\rho c_p)_f}(u_\infty - u)^2 + \frac{16T_\infty^3\sigma^*}{3k^*(\rho c_p)_f}\frac{\partial^2 T}{\partial y^2} + \frac{(\rho c_p)_p}{(\rho c_p)_f}\left[D_\mathrm{B}\frac{\partial C}{\partial y}\frac{\partial T}{\partial y} + \frac{D_\mathrm{T}}{T_\infty}\left(\frac{\partial T}{\partial y}\right)^2\right], \tag{4}$$

$$u\frac{\partial C}{\partial x} + v\frac{\partial C}{\partial y} = D_\mathrm{B}\frac{\partial^2 C}{\partial y^2} + \frac{D_\mathrm{T}}{T_\infty}\frac{\partial^2 T}{\partial y^2}. \tag{5}$$

u and v are fluid velocity components in the x and y directions, υ_f is the kinematic viscosity, k_f is the thermal conductivity, k is the vortex viscosity, ρ_f is the fluid density, N is microrotation or angular velocity, B_0 is the magnetic field, u_∞ is the free stream fluid velocity, T is the fluid temperature, T_∞ is the ambient fluid temperature, μ_f is the dynamic viscosity, $(\rho c_p)_f$ is the heat viscosity of the base fluid, $(\rho c_p)_p$ is the nanoparticle heat capacity, C is the fluid concentration, σ is the electrical conductivity, σ^* is the Stefan–Boltzmann constant, D_B and D_T are the coefficients of Brownian motion and thermophoretic diffusion. The related boundary conditions are

$$\left.\begin{aligned} &y = 0 : u = u_w, \quad v = 0, \quad N = 0, \quad T = T_w \\ &\frac{\partial c}{\partial y} = -\left(\frac{D_\mathrm{T}}{D_\mathrm{B}T_\infty}\right)\frac{\partial T}{\partial y} \\ &y \to \infty : u \to u_\infty, \quad N \to 0 \\ &T \to T_\infty, \quad C \to C_\infty \end{aligned}\right\}. \tag{6}$$

The local similarity transformation regarding this study is as follows:

$$\left.\begin{aligned} &\eta=\sqrt{\frac{b}{\upsilon_f}}y, \quad u=bxf'(\eta), \quad v=-\sqrt{b\upsilon_f}f(\eta) \\ &N=\sqrt{\frac{b^3}{\upsilon_f}}xg(\eta), \quad \theta(\eta)=\frac{T-T_\infty}{T_w-T_\infty}, \quad \phi(\eta)=\frac{C-C_\infty}{C_\infty} \end{aligned}\right\}, \tag{7}$$

where f is the stream function, $\theta(\eta)$ is the dimensionless temperature, T_w is the fluid temperature at the stretching sheet, $\phi(\eta)$ is the dimensionless concentration and C_∞ is the ambient species concentration. We get the following transformed equations and boundary conditions by using similarity transformation (7) in eqs (2)–(5) and boundary constraints (6):

$$(1+K)f'''+ff''-(f')^2+Kg'-M(f'-s)+\lambda\theta+s^2=0, \tag{8}$$

$$\left(1+\frac{K}{2}\right)g''+fg'-f'g-K(2g+f'')=0, \tag{9}$$

$$\frac{1}{\mathrm{Pr}}\left(1+\frac{4}{3}R\right)\theta''+f\theta'+(1+K)\mathrm{Ec}(f'')^2+Nt(\theta')^2M\mathrm{Ec}(f'-s)^2+Nb\theta'\phi'=0, \tag{10}$$

$$\phi''+Lef\phi'+\frac{Nt}{Nb}\theta''=0, \tag{11}$$

$$\left.\begin{aligned} &\eta=0: f(\eta)=0, \quad f'(\eta)=1 \\ &g(\eta)=0, \quad \theta(\eta)=1 \\ &Nb\phi'(\eta)+Nt\theta'(\eta)=0 \\ &\eta\to\infty: f'(\eta)\to s, \quad g(\eta)\to 0 \\ &\theta(\eta)\to 0, \quad \phi(\eta)\to 0 \end{aligned}\right\}, \tag{12}$$

where

$$Le=\frac{\upsilon_f}{D_B}, \quad Nt=\frac{(\rho c_p)_p D_\mathrm{T}(T_w-T_\infty)}{(\rho c_p)_f \upsilon_f T_\infty},$$

$$Nb=\frac{(\rho c_p)_p D_\mathrm{B}(C_\infty)}{(\rho c_p)_f \upsilon_f},$$

$$R=\frac{4T_\infty^3\sigma^*}{k^*k_f}, \quad \mathrm{Re}_x=\frac{u_w x}{\upsilon_f},$$

$$\gamma_f=(\mu_f+k/2)j_f,$$

$$\upsilon_f=\frac{\mu_f}{\rho_f}, \quad K=\frac{k}{(\rho\upsilon)_f}, \quad j_f=\frac{\upsilon_f}{b},$$

$$\mathrm{Gr}_x=\frac{g\beta(T_w-T_\infty)x^3}{\upsilon_f^2},$$

$$\mathrm{Ec}=\frac{{u_w}^2}{c_p(T_w-T_\infty)}, \quad M=\frac{\sigma B^2}{\rho_f b},$$

$$s=a/b, \quad \lambda=\frac{\mathrm{Gr}_x}{\mathrm{Re}_x^2}, \quad \mathrm{Pr}=\frac{\upsilon_f(\rho c_p)_f}{k_f},$$

where K is the material parameter, s is the stretching parameter, R is the radiation parameter, Re_x is the local Reynolds number, Ec is the Eckert number, M is the magnetic parameter, Nt is the thermophoretic parameter, Nb is the Brownian motion parameter, Le is the Schmidt number, β is the thermal expansion coefficient, γ_f is the spin gradient voscosity, j_f is the microinertial density, Gr_x is the local Greshof number, Pr is the Prandtl number, u_w is the stretching velocity, λ is the mixed convection parameter, a and b are arbitrary constants. For engineering point of view, some essential physical quantities, i.e. skin friction coefficient (Cf_x) and local Nusselt number (Nu_x) are defined as follows:

$$Cf_x=\frac{\tau_w}{\rho_f u_w^2}, \quad \mathrm{Nu}_x=\frac{xq_w}{k_f(T_w-T_\infty)}, \tag{13}$$

where τ_w and q_w are the surface shear stress and surface heat flux, respectively, whose mathematical definitions are as follows:

$$\left.\begin{aligned} &\tau_w=\left[(\mu_f+k_f)\frac{\partial u}{\partial y}+kN\right]_{y=0} \\ &q_w=-\left(k_f+\frac{16\sigma^*T_\infty^3}{3k^*}\right)\left(\frac{\partial T}{\partial y}\right)_{y=0} \end{aligned}\right\}. \tag{14}$$

The couple stress at the surface is defined as

$$M_w=\gamma_f\left(\frac{\partial N}{\partial y}\right)_{y=0}. \tag{15}$$

By using similarity transformation (7) into eqs (13)–(15), we have

$$\left.\begin{aligned} &Cf_x\sqrt{\mathrm{Re}_x}=(1+K)f''(0) \\ &M_w=(1+K/2)\mu_f\sqrt{b\upsilon_f\mathrm{Re}_x}g'(0) \\ &\mathrm{Nu}_x\,\mathrm{Re}_x^{-1/2}=-(1+4R/3)\theta'(0) \end{aligned}\right\}. \tag{16}$$

3. Solution methodology

We have used the successive linearisation method (SLM) [40] to solve nonlinear boundary layer equations (8)–(11) along with the boundary conditions

written in eqs (12). For utilising this technique, the functions $f(\eta)$, $g(\eta)$, $\theta(\eta)$ and $\phi(\eta)$ are considered as

$$\left.\begin{aligned} f(\eta) &= f_j(\eta) + \sum_{w=0}^{j-1} F_w(\eta) \\ g(\eta) &= g_j(\eta) + \sum_{w=0}^{j-1} G_w(\eta) \\ \theta(\eta) &= \theta_j(\eta) + \sum_{w=0}^{j-1} \Theta_w(\eta) \\ \phi(\eta) &= \phi_j(\eta) + \sum_{w=0}^{j-1} \Phi_w(\eta) \end{aligned}\right\}, \tag{17}$$

where $F_w(\eta)$, $G_w(\eta)$, $\Theta_w(\eta)$ and $\Phi_w(\eta)$ are successive approximations while functions $f(\eta)$, $g(\eta)$, $\theta(\eta)$ and $\phi(\eta)$ are unknown. We have to make an initial guess that satisfies the boundary conditions for f, g, θ and ϕ. Let the initial guesses be

$$\left.\begin{aligned} &F_0 = 1 - s + s\eta - (1-s)\mathrm{e}^{-\eta}, \quad G_0 = \eta\mathrm{e}^{-\eta} \\ &\Theta_0 = \mathrm{e}^{-\eta}, \quad \Phi_0 = -\frac{Nt}{Nb}\mathrm{e}^{-\eta} \end{aligned}\right\}. \tag{18}$$

By substituting eq. (17) into eqs (8)–(11), we obtain the linearised form of the system of equations. Solving these linearised equations and using the initial guess, we get the corresponding solutions F_j, G_j, Θ_j and Φ_j. The solutions of $f(\eta)$, $g(\eta)$, $\theta(\eta)$ and $\phi(\eta)$ after n iterations can be expressed as

$$\left.\begin{aligned} &f(\eta) \approx \sum_{w=0}^{n} F_w(\eta), \quad g(\eta) \approx \sum_{w=0}^{n} G_w(\eta) \\ &\theta(\eta) \approx \sum_{w=0}^{n} \Theta_w(\eta), \quad \phi(\eta) \approx \sum_{w=0}^{n} \Phi_w(\eta) \end{aligned}\right\}. \tag{19}$$

These linearised equations are solved by using the Chebyshev spectral collocation scheme in which polynomials are defined on $[-1, 1]$ closed interval. Hence, by using the domain truncation method, the domain $[0, \infty)$ is converted to $[-1, 1]$. In this method, the solution of the problem is obtained in the interval $[0, L^*]$ in place of $[0, \infty)$ by utilising the following transformation:

$$\frac{\eta}{L^*} = \frac{\zeta + 1}{2}, \quad -1 \le \zeta \le 1. \tag{20}$$

L^* is called scaling parameter which is very significant due to its use in implementing boundary conditions at infinity. Let P be the number of collocation points and the Gauss–Lobatto collocation point method is used to discretise the domain $[-1, 1]$ which is defined as follows:

$$\zeta = \cos\frac{\pi i}{P}, \quad i = 0, 1, 2, \ldots, P. \tag{21}$$

At these P collocation points the functions F_j, G_j, Θ_j and Φ_j, for $j \ge 1$, are approximated with the help of kth Chebyshev polynomial (T_k^*) as follows:

$$\left.\begin{aligned} F_j(\zeta) &\approx \sum_{k=0}^{P} F_j(\zeta_k) T_k^*(\zeta_k) \\ \Theta_j(\zeta) &\approx \sum_{k=0}^{P} \Theta_j(\zeta_k) T_k^*(\zeta_k) \\ \Phi_j(\zeta) &\approx \sum_{k=0}^{P} \Phi_j(\zeta_k) T_k^*(\zeta_k) \\ G_j(\zeta) &\approx \sum_{k=0}^{P} G_j(\zeta_k) T_k^*(\zeta_k) \end{aligned}\right\}. \tag{22}$$

kth Chebyshev polynomial is defined as

$$T_k^*(\zeta) = \cos[k \cos^{-1}(\zeta)]. \tag{23}$$

The rth derivative of functions at the collocation points F_j, G_j, Θ_j and Φ_j is constructed as

$$\left.\begin{aligned} \frac{\mathrm{d}^r F_j}{\mathrm{d}\eta^r} &= \sum_{k=0}^{P} S_{ki}^r F_j(\zeta_k), \quad \frac{\mathrm{d}^r \Theta_j}{\mathrm{d}\eta^r} = \sum_{k=0}^{P} S_{ki}^r \Theta_j(\zeta_k) \\ \frac{\mathrm{d}^r G_j}{\mathrm{d}\eta^r} &= \sum_{k=0}^{P} S_{ki}^r G_j(\zeta_k), \quad \frac{\mathrm{d}^r \Phi_j}{\mathrm{d}\eta^r} = \sum_{k=0}^{P} S_{ki}^r \Phi_j(\zeta_k) \end{aligned}\right\}. \tag{24}$$

Here $S = 2D/L^*$, where D is the Chebyshev differentiation matrix and the entries of this matrix are as follows:

$$\begin{aligned} &D_{00} = \frac{2P^2+1}{6}, \quad D_{ik} = \frac{c_i(-1)^{i+k}}{c_k\zeta_i - \zeta_k}, \\ &\quad i \ne k; i, k = 0, 1, \ldots, P, \\ &D_{PP} = -\frac{2P^2+1}{6}, \quad D_{kk} = -\frac{\zeta_k}{2(1-\zeta_k^2)}, \\ &\quad k = 1, 2, \ldots, P-1. \end{aligned} \tag{25}$$

In this procedure, we get the following matrix equation:

$$A_{j-1} X_j = R_{j-1}, \tag{26}$$

where A_{j-1} is a $(4P+4) \times (4P+4)$ square matrix and X_j and R_{j-1} are $(4P+4) \times 1$ column vectors, defined by

Table 1. Comparison of $-f''(0)$ and $g'(0)$ vs. M and K at Pr $= 0.71$, Ec $= 0.02$ and $Le = 0.2$ with Eldabe and Ouaf [41].

M	K	Present $-f''(0)$	Ref. [41] $-f''(0)$	Present $g'(0)$	Ref. [41] $g'(0)$
0		0.9097374	0.9097610	0.09499677	0.09500014
0.5		1.11437537	1.11437433	0.10508993	0.10508899
1		1.28713481	1.28710689	0.11212551	0.11212436
	0	1.41421356	1.41421366	0	0
	0.5	1.14076562	1.14073597	0.2111671	0.21116566
	2	0.76966611	0.76957791	0.35855446	0.35855041

$$A_{j-1} = \begin{bmatrix} A_{11} & A_{12} & A_{13} & A_{14} \\ A_{21} & A_{22} & A_{23} & A_{24} \\ A_{31} & A_{32} & A_{33} & A_{34} \\ A_{41} & A_{42} & A_{43} & A_{44} \end{bmatrix}, \quad x_j = \begin{bmatrix} F_j \\ \Theta_j \\ \Phi_j \\ G_j \end{bmatrix},$$

$$R_{j-1} = \begin{bmatrix} r_{1,j-1} \\ r_{2,j-1} \\ r_{3,j-1} \\ r_{4,j-1} \end{bmatrix}, \tag{27}$$

where

$$F_j = [f_j(\zeta_0), f_j(\zeta_1), \ldots, f_j(\zeta_{P-1}), f_j(\zeta_P)]^{\mathrm{T}},$$

$$\Theta_j = [\theta_j(\zeta_0), \theta_j(\zeta_1), \ldots, \theta_j(\zeta_{P-1}), \theta_j(\zeta_P)]^{\mathrm{T}},$$

$$\Phi_j = [\phi_j(\zeta_0), \phi_j(\zeta_1), \ldots, \phi_j(\zeta_{P-1}), \phi_j(\zeta_P)]^{\mathrm{T}},$$

$$G_j = [g_j(\zeta_0), g_j(\zeta_1), \ldots, g_j(\zeta_{P-1}), g_j(\zeta_P)]^{\mathrm{T}},$$

$$r_{1,j-1} = [r_{1,j-1}(\zeta_0), r_{1,j-1}(\zeta_1), \ldots, r_{1,j-1}(\zeta_P)]^{\mathrm{T}},$$

$$r_{2,j-1} = [r_{2,j-1}(\zeta_0), r_{2,j-1}(\zeta_1), \ldots, r_{2,j-1}(\zeta_P)]^{\mathrm{T}},$$

$$r_{3,j-1} = [r_{3,j-1}(\zeta_0), r_{3,j-1}(\zeta_1), \ldots, r_{3,j-1}(\zeta_P)]^{\mathrm{T}},$$

$$r_{4,j-1} = [r_{4,j-1}(\zeta_0), r_{4,j-1}(\zeta_1), \ldots, r_{4,j-1}(\zeta_P)]^{\mathrm{T}},$$

$$A_{1,1} = a_{1,j-1}D^3 + a_{2,j-1}D^2 + a_{3,j-1}D + a_{4,j-1}I,$$

$$A_{1,2} = a_{5,j-1}I, \quad A_{1,3} = O, \quad A_{2,2} = b_{4,j-1}I,$$

$$A_{1,4} = a_{6,j-1}D, \ A_{2,1} = b_{1,j-1}D^2 + b_{2,j-1}D + b_{3,j-1}I,$$

$$A_{2,3} = b_{5,j-1}I, \ A_{2,4} = b_{6,j-1}D^2 + b_{7,j-1}D + b_{8,j-1}I,$$

$$A_{3,1} = c_{1,j-1}D^2 + c_{2,j-1}D + c_{3,j-1}I,$$

$$A_{3,2} = c_{4,j-1}D^2 + c_{5,j-1}D + c_{6,j-1}I,$$

$$A_{3,3} = c_{7,j-1}D, \ A_{3,4} = c_{8,j-1}I, \ A_{4,1} = d_{1,j-1}I,$$

$$A_{4,3} = d_{3,j-1}D^2 + d_{4,j-1}D,$$

$$A_{4,4} = O, \ A_{4,2} = d_{2,j-1}D^2.$$

4. Validation of approximate solution

In order to justify our results, we have carried out a comparison in the limiting sense between our results and the results obtained by Eldabe and Ouaf [41]. Table 1 presents the comparison of—$f''(0)$ and $g'(0)$ vs. M and K when Pr $= 0.71$, Ec $= 0.02$, $Le = 0.2$ with Eldabe and Ouaf [41]. Good agreement between them can be seen from table 1 that leads to justify the present analysis.

5. Results and discussion

The present analysis deals with the stagnation point flow of micropolar nanofluid over a stretching surface. We have analysed and plotted the angular velocity, temperature, velocity and concentration profiles by varying various active parameters. For numerical computation, we have taken $Le = 1.5$, $\lambda = 10$, $Nb = 0.2$, $Nt = 0.1$, Ec $= 0.2$, Pr $= 6.7$, $R = 1$, $s = 0.5$, $M = 5$ and $K = 1.5$ as default values, until otherwise specified particularly. Each figure contains two sets of curves, i.e. dash line and solid line, and they simultaneously represent a particular graph for two disparate values of parameters specified within the figure.

5.1 *Micropolar nanofluid velocity profile*

Figures 2–5 are the micropolar fluid velocity profiles for different values of flow parameter specified within the figure. Velocity profile for disparate values of stagnation parameter along with mixed convection parameter is shown in figure 2. The ratio of free stream velocity and stretching sheet velocity is called stagnation parameter. When $s < 1$ the stretching sheet velocity is greater than free stream velocity and when $s > 1$ the free stream is moving faster than the stretching sheet. From figure 2, it can be observed that increment in s leads to an increase in fluid velocity. It is worth pointing out that when $s = 1$ and when there is no convection, there is no boundary

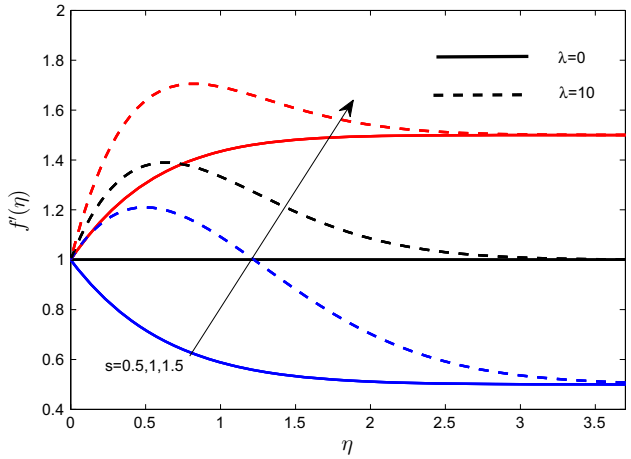

Figure 2. Velocity profile for s.

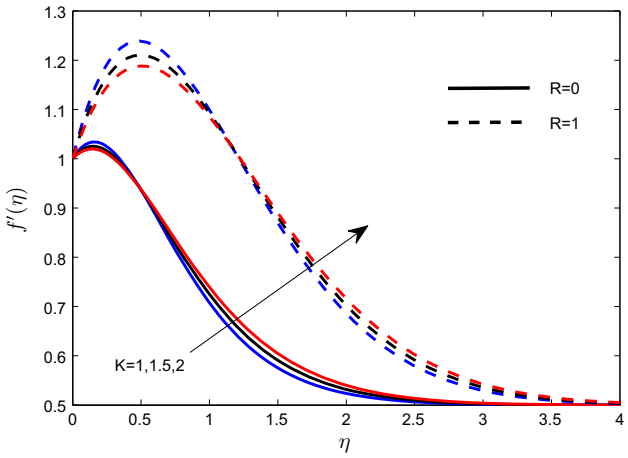

Figure 4. Velocity profile for K.

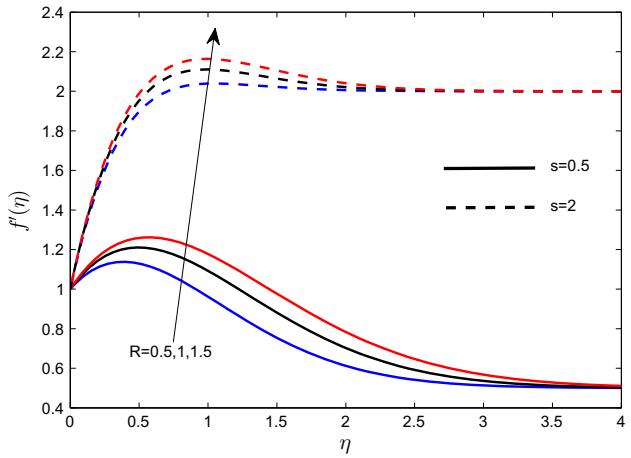

Figure 3. Velocity profile for R.

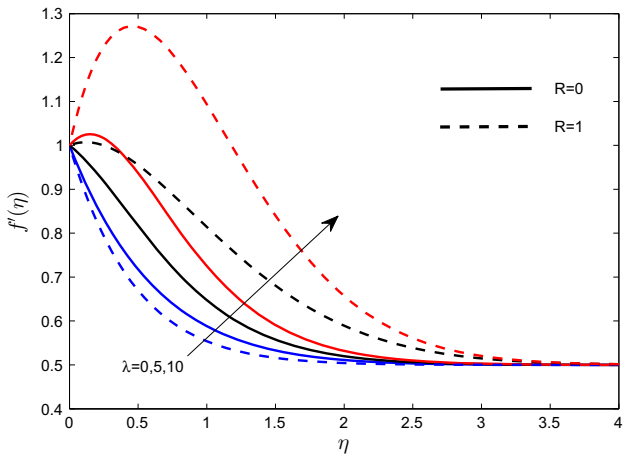

Figure 5. Velocity profile for λ.

layer formation but boundary layer is formed in the presence of mixed convection parameter. This variation is encountered due to the contribution of buoyancy force acting on the fluid flow which assists the fluid motion and increases the velocity profile. The velocity profile for different values of radiation parameter in both cases, i.e. $s < 1$ and $s > 1$, is shown in figure 3. Enhancement in the radiation parameter leads to increase in fluid velocity. This is due to the fact that pressure gradient increases with the increment in radiation parameter which assists the fluid motion. Figure 4 shows the effect of microrotation parameter in the absence and in the presence of radiation parameter. A higher microrotation parameter leads to a decrease in the viscosity of the fluid. Therefore, in both cases, the velocity distribution initially decreases but as it approaches free stream, it starts increasing. The effect of mixed convection parameter on the velocity profile in the presence and in the absence of radiation parameter is shown in figure 5. Since the ratio of buoyancy force to inertia force is the mixed convection parameter, it is observed that the increment in λ boosts the velocity profile due to the strengthening of thermal buoyancy force. It is also seen that the presence of radiation parameter will strengthen this phenomenon.

5.2 *Micropolar nanofluid temperature profile*

The influence of some flow parameters on micropolar fluid temperature profile is shown in figures 6–8. It can be seen from figure 6 that the increment in Ec leads to an increase in the temperature profile which is practically true because Ec comes from taking viscous and Joule dissipation terms into account. For higher Ec, the friction force produces more heat between fluid particles. Therefore, an increment in Ec leads to an increase in kinetic energy which helps to raise the temperature of the fluid. It can be seen from figure 6 that when $R = 0$, the temperature increases with increment in Ec and when $R = 1$, same but slightly stronger phenomenon is observed. Figure 7 shows the temperature profile for different values of R in the presence and in the absence of K. Generally, it is noted that more heat is

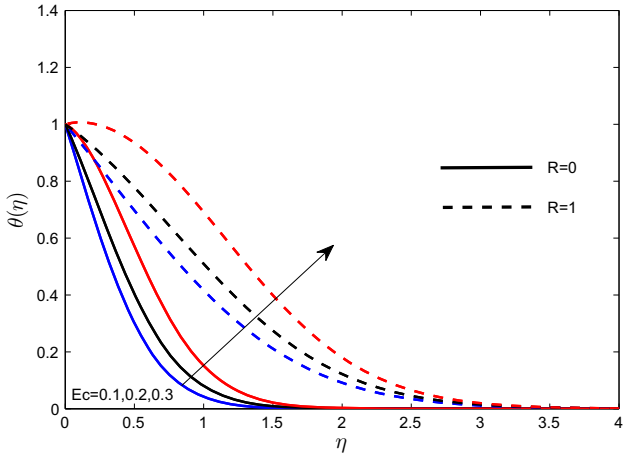

Figure 6. Temperature profile for Ec.

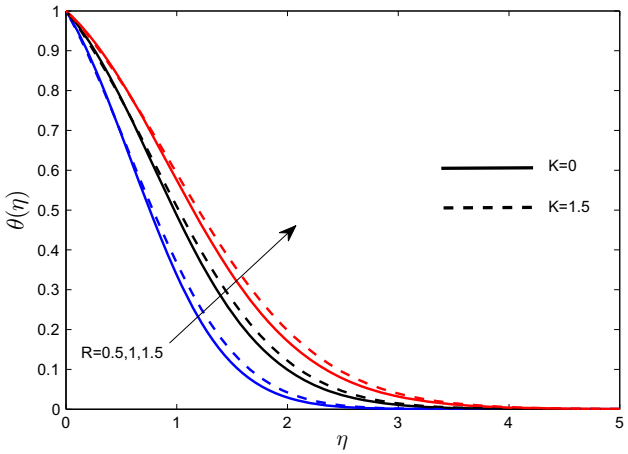

Figure 7. Temperature profile for R.

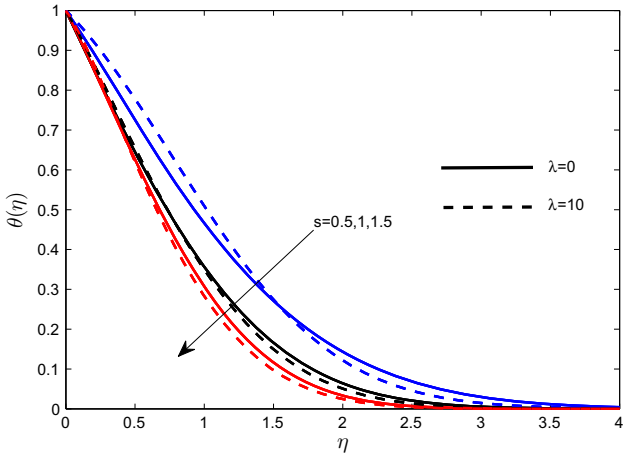

Figure 8. Temperature profile for s.

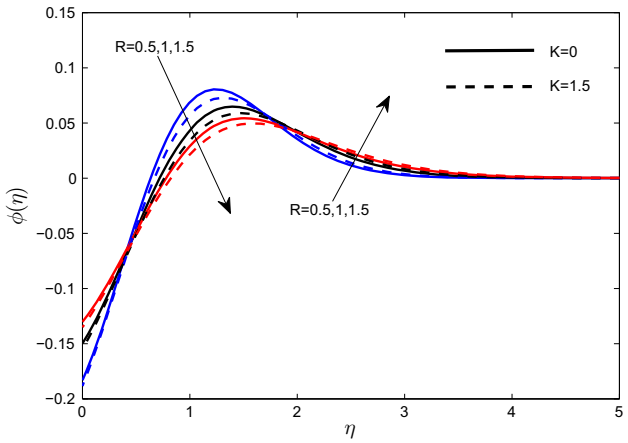

Figure 9. Concentration profile for R.

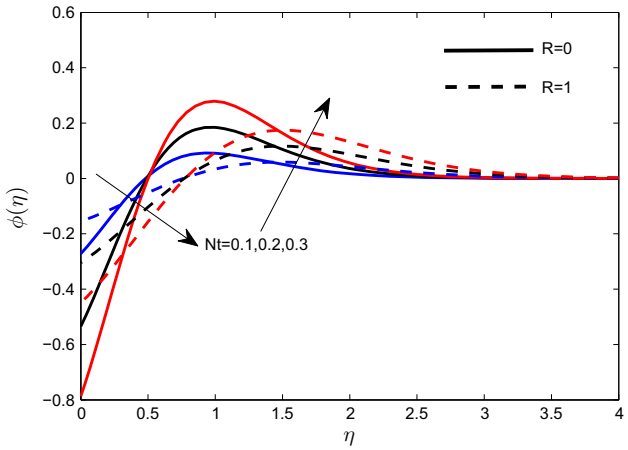

Figure 10. Concentration profile for Nt.

absorbed by the fluid in the presence of thermal radiation, and so due to temperature gradient, diffusion flux occurs. Therefore, an increment in fluid temperature and thermal boundary layer thickness can be noticed with an increment in radiation parameter. It is also noticed that in the case of micropolar fluid, the boundary layer becomes thicker which is solely the contribution of high orientation of fluid particles in micropolar fluids. It is shown in figure 8 that the increment in stagnation parameter leads to decrease in the fluid temperature throughout the boundary layer in the absence and in the presence of buoyancy force.

5.3 *Micropolar nanofluid concentration profile*

Figures 9–11 show the influence of some active flow parameters on micropolar fluid concentration profile. Figure 9 shows the radiation effect on concentration profile. Generally, it is to be noted that enhancement in the radiation parameter increases the pressure gradient and diffusion flux. Significantly, increment in R initially reduces the concentration and as going away from the sheet, the concentration tends to increase. It is also observed here that this effect is stronger in Newtonian fluid than in micropolar fluid. Figure 10 shows the

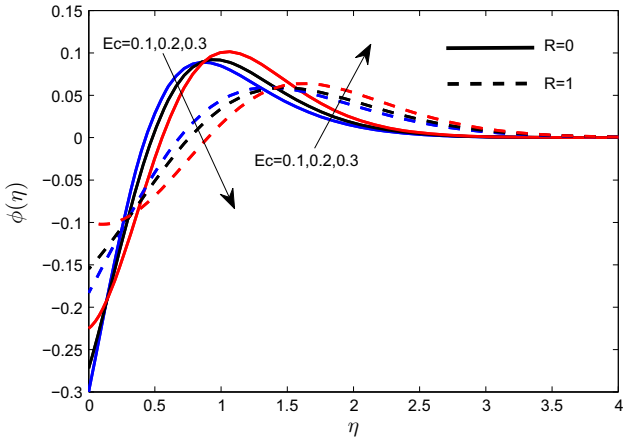

Figure 11. Concentration profile for Ec.

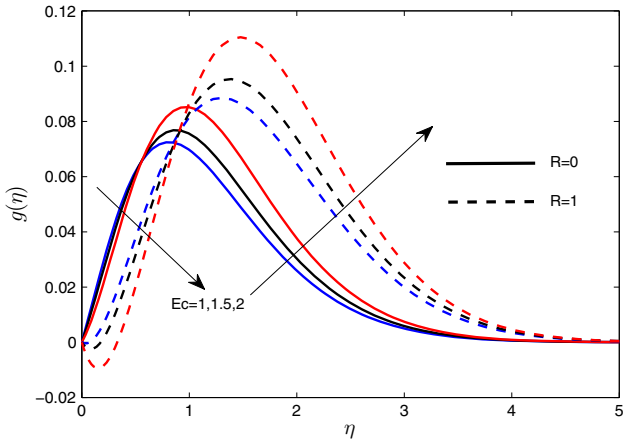

Figure 12. Angular velocity profile for Ec.

nanoparticle concentration profile for different values of Nt in the presence and in the absence of R. It can be seen that increment in Nt enhances the concentration profile because nanoparticles move from the hot surface to the cold surface due to thermophoretic diffusion. As a result, nanoparticle volume fraction hikes up. Figure 11 shows the nanoparticle concentration profile for various values of Ec in the presence and in the absence of thermal radiation as Ec has a tendency to create obstacle in the migration of nanoparticles within the boundary layer. So, it can be noticed from figure 11 that concentration decreases rapidly in the central area of the boundary layer with an increment in Ec. This phenomenon gets reversed when going away from the mid-region of the boundary layer.

5.4 *Micropolar nanofluid angular velocity profile*

Figures 12–15 show the micropolar fluid angular velocity profiles for different values of some parameters. As Ec has a tendency to create obstacle in the migration of nanoparticles and for higher Ec, the friction force produces more heat between fluid particles, from figure 12, it can be seen that initially, angular velocity decreases near the sheet but as the fluid moves away from the

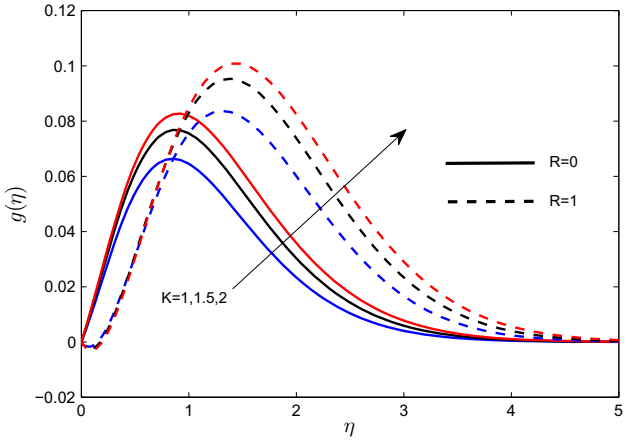

Figure 13. Angular velocity profile for K.

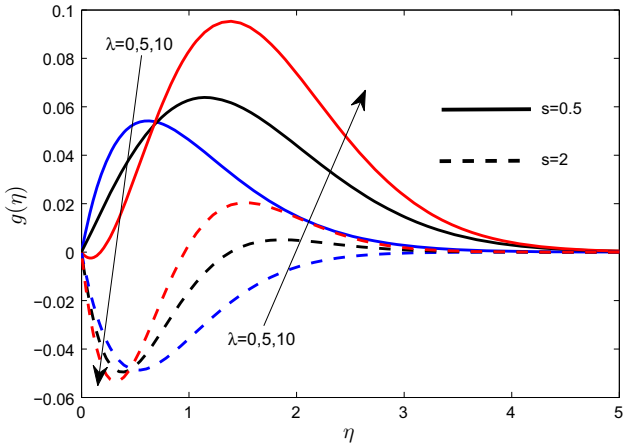

Figure 14. Angular velocity profile for λ.

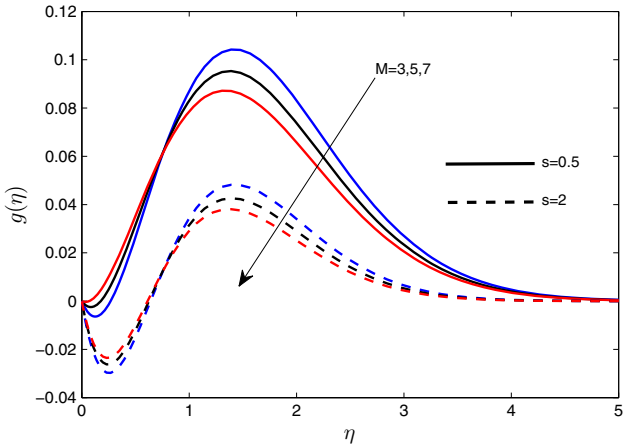

Figure 15. Angular velocity profile for M.

Table 2. Values of $f''(0)$, $\theta'(0)$, $\phi'(0)$ and $g'(0)$ for the specified parameters.

M	Le	Nt	Ec	R	λ	s	K	$f''(0)$	$\theta'(0)$	$g'(0)$
3								1.63981314	− 0.58480354	− 0.23674624
5								1.51811813	− 0.59324065	− 0.20872138
7								1.41899736	− 0.6025444	− 0.18662494
	1							1.51656149	− 0.5958223	− 0.20832849
	1.5							1.51811813	− 0.59324065	− 0.20872138
	2							1.51922382	− 0.59132209	− 0.20898913
		0.1						1.51811813	− 0.59324065	− 0.20872138
		0.2						1.52647216	− 0.58044546	− 0.21102056
		0.3						1.53492739	− 0.56755113	− 0.21335809
			0.1					1.47494319	− 0.71639432	− 0.19841286
			0.2					1.51811813	− 0.59324065	− 0.20872138
			0.3					1.57350906	− 0.44024898	− 0.22200365
				0.5				1.33969731	− 0.8186771	− 0.15886828
				1				1.51811813	− 0.59324065	− 0.20872138
				1.5				1.62344035	− 0.48532456	− 0.24236254
					0			0.30239451	− 0.74582697	− 0.04263556
					5			0.75048572	− 0.72468254	− 0.10405172
					10			1.51811813	− 0.59324065	− 0.20872138
						0.5		0.96222389	− 0.33680301	− 0.06124082
						1		1.51811813	− 0.59324065	− 0.20872138
						1.5		2.32344341	− 0.48222147	− 0.4085853
							1	1.13840569	− 0.32788579	− 0.04921112
							1.5	0.96222389	− 0.33680301	− 0.06124082
							2	0.83547991	− 0.34362789	− 0.06744872

Table 3. Quadratic regression coefficients and error bound for the estimated $Cf_x\sqrt{\mathrm{Re}_x}$.

s	CF	a_1	a_2	a_3	a_4	a_5	ε_1
0.5	− 1.03164	0.12241	0.23391	0.03316	0.00236	− 0.05503	4.81×10^{-4}
0.7	− 0.61213	0.0457	0.22365	0.02564	9.81×10^{-5}	− 0.03231	0.0029
1.2	0.63531	− 0.34899	0.2221	0.10243	− 0.04890	− 0.04374	0.0069

sheet, this effect is reversed. It is also noticed that radiation parameter assists angular velocity distribution and increases boundary layer width. Figure 13 shows the angular velocity profile for disparate values of K in the presence and in the absence of radiation parameter. It can be noticed from figure 13 that an increment in K leads to an increase in angular velocity in both the cases of radiation but this phenomenon is stronger in the presence of radiation. In figure 14, it can be seen that when $s < 1$ the increment in λ initially reduces the angular velocity and as the fluid moves away from the sheet, angular velocity tends to increase due to the buoyancy force. This phenomenon is totally reversed when $s > 1$ due to boundary layer reversal.

The angular velocity profiles for disparate values of M and s are shown in figure 15. It is observed that when $s < 1$, the angular velocity increases near the sheet and as the fluid moves away from it, angular velocity profiles start decreasing with the increment in M. When $s > 1$, angular velocity profiles decrease with an increment in M, which is practically true because electromagnetic body force slows down the momentum for the flow field, and therefore angular velocity is observed to decrease.

5.5 *Skin friction, Nu_x and couple stress at the surface*

Numerical values of skin friction coefficient, $\mathrm{Nu_x}$ and couple stress at the surface, corresponding to active flow parameters, are given in table 2. From table 2, it is suggested that an increment in Le, Nt, Ec and λ leads to enhanced skin friction and couple stress at the surface in magnitude but they have reverse impact on rate of heat transfer. Parameters M and K have the tendency to increase heat transfer rate but they have reverse effect on skin friction. Parameter M has the tendency to reduce the couple stress at the surface. However, parameter K increases it. Parameters R and s have the tendency to

increase skin friction and couple stress at the surface. However, parameter R decreases the heat transfer rate. When $s \leq 1$, parameter s has the tendency to increase heat transfer rate but when $s > 1$, it shows exactly the opposite nature.

6. Quadratic multiple regression model for the statistical analysis of skin friction coefficient

In this section, a quadratic multiple regression method is used to perform the statistical analysis of skin friction coefficient corresponding to some dominating flow parameters. For analysing skin friction, we have taken fixed values of s and the values of M and λ generated randomly from the set of 100 values chosen from the intervals (0.5, 5) and (5, 15). The approximated quadratic regression model for $Cf_x\sqrt{\mathrm{Re}_x}$ is given as follows:

$$Cf_{\mathrm{est}} = Cf + a_1\lambda + a_2K + a_3\lambda^2 + a_4K^2 + a_5\lambda K. \tag{28}$$

The maximum relative error is calculated by

$$\varepsilon_1 = |Cf_{\mathrm{est}} - Cf|/|Cf|. \tag{29}$$

All the regression coefficients along with maximum relative error in this estimation are given in table 3. It can be observed from table 3 that when $s = 0.5$ and 0.7, the coefficient of λ is less than the coefficient of K, indicating that small variation in K leads to large perturbation in $Cf_x\sqrt{\mathrm{Re}_x}$ in comparison to mixed convection parameter, whereas when $s = 1.2$, parameter λ becomes more dominant.

7. Conclusion

Some significant findings of the present investigation are as follows:

- The increment in parameters Le, Nt, Ec and λ enhances the magnitude of skin friction and couple stress at the surface, but they have reverse impact on the rate of heat transfer. Parameters R and s have the tendency to increase skin friction and couple stress at the surface, but parameter R decreases the heat transfer rate.
- Stagnation, radiation and mixed convection parameters enhance the velocity profile. Microrotation parameter reduces it near the sheet and the reverse trend is observed away from the sheet.
- Ec and radiation parameter have the tendency to boost temperature distribution but stagnation parameter has reverse impact on it.
- The increment in Ec and radiation parameter leads to decrease in concentration near the sheet but towards free stream, this effect is reversed. The increment in Nt increases concentration of fluid throughout the boundary layer.
- When $s > 1$, parameter M has the tendency to decrease angular velocity. Parameter Ec decreases angular velocity near the surface but reverse trend is observed away from the sheet.
- In the absence of mixed convection parameter, when $s = 1$, boundary layer formation is not observed but in the presence of mixed convection parameter, boundary layer formation is observed. On the other hand, when $s < 1$ increment in λ initially decreases angular velocity but as free stream is approached, angular velocity tends to increase while for $s > 1$ a totally reversed phenomenon is observed.
- From quadratic multiple regression analysis, it is observed that when $s < 1$ small variation in K leads to large perturbation in skin friction in comparison to λ but when $s > 1$, parameter λ becomes more dominant.

References

[1] S U S Choi and J A Eastman, No. ANL/MSD/CP-84938; CONF-951135-29 (Argonne National Lab, IL, USA, 1995)
[2] H Masuda, A Ebata and K Teramae, *Netsu Bussei* **7**, 227 (1993)
[3] J Buongiorno *J. Heat Transf.* **128**, 240 (2006)
[4] A V Kuznetsov and D A Nield, *Int. J. Heat Mass Transf.* **65**, 682 (2013)
[5] S K Das, S U S Choi, W Yu and T Pradeep, *Nanofluids: Science and technology* (John Wiley and Sons, Inc., Hoboken, New Jersey, 2007)
[6] S Kakac and A Pramuanjaroenkij, *Int. J. Heat Mass Transf.* **52**, 3187 (2009)
[7] J A Esfahani, M Akbarzadeh, S Rashidi, M A Rosen and R Ellahi, *Int. J. Heat Mass Transf.* **109**, 1162 (2017)
[8] G S Seth, B Kumar and R Nandkeolyar, *J. Nanofluids* **8**, 620 (2019)
[9] S Rashidi, S Akar, M Bovand and R Ellahi, *Renew. Energy* **115**, 400 (2018)
[10] T Hayat, M Waqas, S A Shehzad and A Alsaedi, *Pramana – J. Phys.* **86**, 3 (2016)
[11] A C Eringen, *J. Math. Mech.* **16**, 1 (1966)
[12] A C Eringen, *J. Math. Anal. Appl.* **38**, 480 (1972)
[13] G Lukaszewicz, *Micropolar fluids: Theory and applications* (Springer Science and Business Media, 1999)
[14] A Mohammadein and R S R Gorla, *Int. J. Numer. Method Heat Fluid Flow* **11**, 50 (2001)
[15] F Ibrahim, I Hassanien and A Bakr, *J. Appl. Mech.* **72**, 468 (2005)

[16] M Sheikholeslami, M Hatami and D Ganji, *J. Mol. Liq.* **194**, 30 (2014)
[17] M J Uddin, M N Kabir and Y M Alginahi, *Comput. Math. Appl.* **70**, 846 (2015)
[18] S Iram, M Nawaz and A Ali, *Pramana – J. Phys.* **91**: 47 (2018)
[19] L J Crane, *Z. Angew. Math. Phys.* **21**, 645 (1970)
[20] R Kandasamy, P Loganathan and P P Arasu, *Nucl. Eng. Des.* **241**, 2053 (2011)
[21] M Turkyilmazoglu, *Int. J. Nonlinear Mech.* **83**, 59 (2016)
[22] K L Hsiao, *Int. J. Heat Mass Transf.* **112**, 983 (2017)
[23] A A Afify and M A El-Aziz, *Pramana – J. Phys.* **88**: 31 (2017)
[24] K Khanafer, K Vafai and M Lightstone *Int. J. Heat Mass Transf.* **46**, 3639 (2003)
[25] I Hassanien, A Essawy and N Moursy, *Appl. Math. Comput.* **152**, 323 (2004)
[26] O D Makinde, W A Khan and Z H Khan, *Int. J. Heat Mass Transf.* **62**, 526 (2013)
[27] M Waqas, M Farooq, M I Khan, A Alsaedi, T Hayat and T Yasmeen, *Int. J. Heat Mass Transf.* **102**, 766 (2016)
[28] K Das, *Comput. Math. Appl.* **63**, 255 (2012)
[29] G Bourantas and V C Loukopoulos, *Int. J. Heat Mass Transf.* **68**, 35 (2014)
[30] N Bachok, A Ishak and I Pop, *Nanoscale Res. Lett.* **6**, 623 (2011)
[31] W Ibrahim, B Shankar and M M Nandeppanavar, *Int. J. Heat Mass Transf.* **56**, 1 (2013)
[32] A Mahmood, B Chen and A Ghaffari, *J. Magn. Magn. Mater.* **416**, 329 (2016)
[33] G S Seth, M K Mishra and R Tripathi, *Comput. Appl. Math.* **37**, 4081 (2018)
[34] E Azhar, Z Iqbal, S Ijaz and E N Maraj, *Pramana – J. Phys.* **91**: 61 (2018)
[35] Y J Kim and A G Fedorov, *Int. J. Heat Mass Transf.* **46**, 1751 (2003)
[36] D Pal and G Mandal, *Int. J. Mech. Sci.* **126**, 308 (2017)
[37] S Siddiqa, A Faryad, N Begum, M A Hossain and R S R Gorla, *Int. J. Therm. Sci.* **111**, 215 (2017)
[38] T Hayat, M I Khan, M Waqas, A Alsaedi and M I Khan, *Int. J. Hydrogen Energy* **42**, 16821 (2017)
[39] A V Kuznetsov and D A Nield, *Int. J. Therm. Sci.* **77**, 126 (2014)
[40] S S Motsa and P Sibanda, *Comput. Math. Appl.* **63**, 1197 (2012)
[41] N T Eldabe and M E Ouaf, *Appl. Math. Comput.* **177**, 561 (2006)